



Interaction of Sea Surface Ice Floes in Fluid Dynamical Eddy Simulations

Jacinta M. K. Clay

Advisor: Baylor Fox-Kemper

Readers: Jung-Eun Lee, Amanda Lynch

*A thesis submitted in partial fulfillment of the requirements for the degree of
Sc.B. with honors in Geology-Physics/Mathematics*

Department of Earth, Environmental, and Planetary Sciences
Brown University

May 2019

Abstract

The thermohaline instabilities imposed by sea ice floes on the surface ocean create submesoscale eddies which are poorly modelled in modern oceanographic or atmospheric models. This work compares a simple two-dimensional diffusive model to the MITgcm's three-dimensional shelf-ice functionality when calculating the change in ocean temperature variance over time.

A rough parameterization of the time required to equilibrate the ice-perturbed ocean according to the MITgcm can be derived by applying the MATLAB model with a diffusive constant equal to the MITgcm eddy diffusivity constant. This can be further crudely parameterized by analyzing the initial conditions of the surface ocean and relating one of two short algorithms described in-text. The eddy diffusivity, κ , of the MITgcm was calculated by comparing the two models and found to exist $\mathcal{O}(10^3)$, though $\kappa = f(\sigma)$. κ varied somewhat with the complexity of the initial sea ice floe arrangement but remained within the order of magnitude.

Contents

1	Introduction	2
1.1	Importance of Sea Ice to the Earth and Environment	2
1.2	Sea Ice Modelling	6
2	Non-Dimensional Sea Ice Counting	7
2.1	Heat Equation	7
2.2	Description of the Toy Model	7
2.3	Central Ice Floes of Increasing Diameter	9
2.4	An example of an ocean with 10 circular ice floes of pre-determined radii	10
2.5	An example of an ocean with 4 circular ice floes of randomized radii	14
3	Utilizing the MITgcm	15
3.1	Description of the Model	15
3.2	Idealized One-Dimensional Floes	15
3.3	More Complex Geometries	20
3.4	Comparing the Toy Model and the MITgcm	24
4	Conclusions	28
	References	38

Chapter 1

Introduction

1.1 Importance of Sea Ice to the Earth and Environment

Presently, recurring sea ice covers 15% of the global ocean, an area equivalent to twice the surface area of North America. Though predominately seasonal, sea ice is fundamental to basin-wide ocean circulation, global energy balance and the continuation of a multitude of cultures and ecosystems that rely on sea ice for nutrition, transportation or enrichment.

Increases in global atmospheric and oceanic heat content, attributable to anthropogenic increases in CO_2 , have caused a decrease in northern hemispheric sea ice thickness and extent (Fig 1.1). The southern sea ice extent has not undergone a similar reduction as can be seen in Fig. 1.2, potentially because of the Southern ocean's response to the thermohaline impacts of melting sea ice (J. Zhang, 2007).

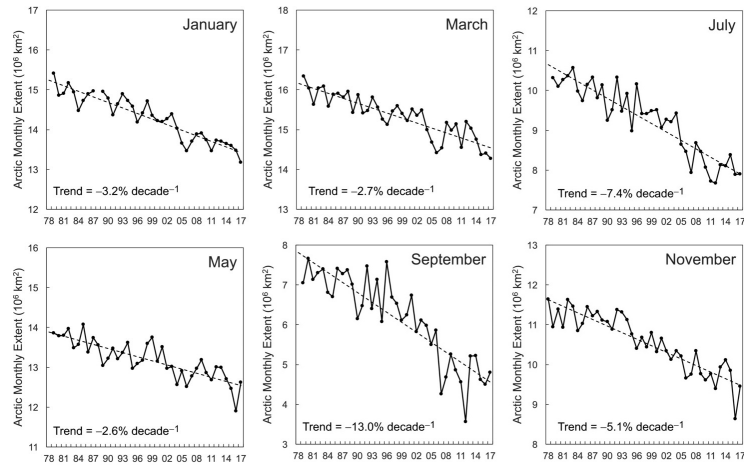


Figure 1.1: Monthly Arctic sea ice extent derived from the passive satellite record. Adapted from Serreze and Meier, 2019.

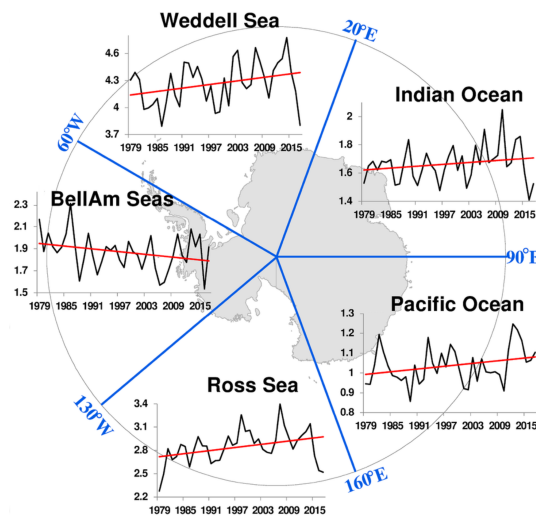


Figure 1.2: Observed Antarctic sea ice extent for five separate oceanographic regions¹. Adapted from Ludescher et al., 2018.

Climate Impacts of Sea Ice Loss

The thickness and area of sea ice strongly affects the global energy budget, since sea ice has a much higher albedo than the surrounding ocean (Curry, Schramm, & Ebert, 1995). Sea ice has the capacity to exacerbate global climate feedbacks as both proxy data and models have indicated that that abrupt climate changes in Earth's history have been sustained or compounded by sea ice dynamics (de Vernal, Gersonde, Goosse, Seidenkrantz, & Wolff, 2013; Dokken, Nisancioglu, Li, Battisti, & Kissel, 2013; Z. Zhang, Nisancioglu, & Ninnemann, 2013; Born, Nisancioglu, & Risebrobakken, 2011).

Additionally, sea ice modulates global climate by perpetuating deep ocean circulation (Ferrari et al., 2014; Goosse & Fichefet, 1999). Since salt water is more difficult to freeze than freshwater, sea ice emits salt as it freezes, which concentrates the salinity and density of nearby water. This density causes the water to descend to the ocean basin, which powers Meridional Overturning Circulation (Marshall & Speer, 2012). A weakening in seasonal sea ice is theorized to cause a reduction in Atlantic Meridional Circulation, which would have climatic, ecological and economic impacts for the states neighboring the Gulf Stream as well as the populations of Western Europe (Pohlmann, Sienz, & Latif, 2006; Cunningham et al., 2010).

¹Several climate skeptics have used the apparent ambiguity of the southern hemisphere sea ice extent to claim that anthropogenic climate change is less serious than climate scientists warn. A proper rebuttal to that argument can be found in *Increasing Antarctic Sea Ice under Warming Atmospheric and Oceanic Conditions* (J. Zhang, 2007)

Ecological Impacts of Sea Ice Loss

Sea ice is a strong determinant of the biota of the polar oceans (Fig. 1.3). Archaea, bacteria and eukarya have been observed in sea ice environments and the thickness of sea ice dictates whether phototrophy or chemotrophy fuels the producers within the food chain (Boetius, Anesio, Deming, Mikucki, & Rapp, 2015). These microorganisms form ecosystems as abundant as those found in freshwater systems and cryospheric changes such as those resulting from anthropogenic climate change threaten major shifts in the populations, distributions and life processes of cold-adapted microorganisms as well as the biogeochemical processes and species that depend upon them (Boetius et al., 2015; Post et al., 2013). Sea ice algae provide 57% of the primary production of the central Arctic and is dependent on seasonally thinning sea ice for timing its annual bloom (Gosselin, Levasseur, Wheeler, Horner, & Booth, 1997; Post et al., 2013).

Because sea ice bridges terrestrial and ocean environs, sea ice loss threatens an environment used by flora and fauna alike to breed, hunt, hide, rest, socialize, or care for young (Post et al., 2013). The most infamous example is the growing endangerment of polar bears, symbolic of all those vulnerable to climate change. Polar bears depend on sea ice for hunting seals and other prey; consequently populations of polar bears have been strongly linked with local sea ice extent (Derocher, Lunn, & Stirling, 2004; Regehr, Hunter, Caswell, Amstrup, & Stirling, 2010). A schematic illustrating some of the ecological impacts of sea ice loss can be seen in Fig. 1.3.

Cultural and Economic Impacts of Sea Ice Loss

Unlike land ice, melting sea ice does not contribute to rising sea levels, though the resulting impact on global albedo would perpetuate the global energy imbalance which is estimated to displace 2.4% of the world's population by 2100 (Nicholls et al., 2011). Moreover, decreases in sea ice thickness and extent can cause cultural or economic disruption when cultures or economies depend on sea ice for social, agricultural or transportation needs. In example, the potential extinction of the polar bear threatens the economies of indigenous polar bear hunting, non-indigenous conservation hunting, and non-indigenous polar-bear-watching, and the severance of each economy would impact locals and non-locals alike (Lemelin, 2006). The melt of sea ice (independent of all consequent climate changes) would have the greatest impact on indigenous Arctic communities, which are poorly represented in international geopolitics (Berkes & Jolly, 2002; Roosvall & Tegelberg, 2015).

Additionally there are some communities that may benefit from a decrease in northern hemispheric sea ice extent. Decreases in sea ice may, somewhat ironically, make arctic oil more accessible to offshore drillers, which has economic implications for Arctic countries with claim to this oil as well as the non-Arctic countries with historical or financial investment in the oil industry, such as the United States of America (Gautier et al., 2009; Comfort, Dinovitzer, Lazor, & Hinnah, 2004). An ice-less Arctic will also allow for new travel and trade routes between the Arctic countries which has social, cultural, economic, political and militaristic implications (Backus & Strickland, 2008; Dodds, 2008; Humpert & Raspotnik, 2012; Ebinger & Zambetakis, 2009)

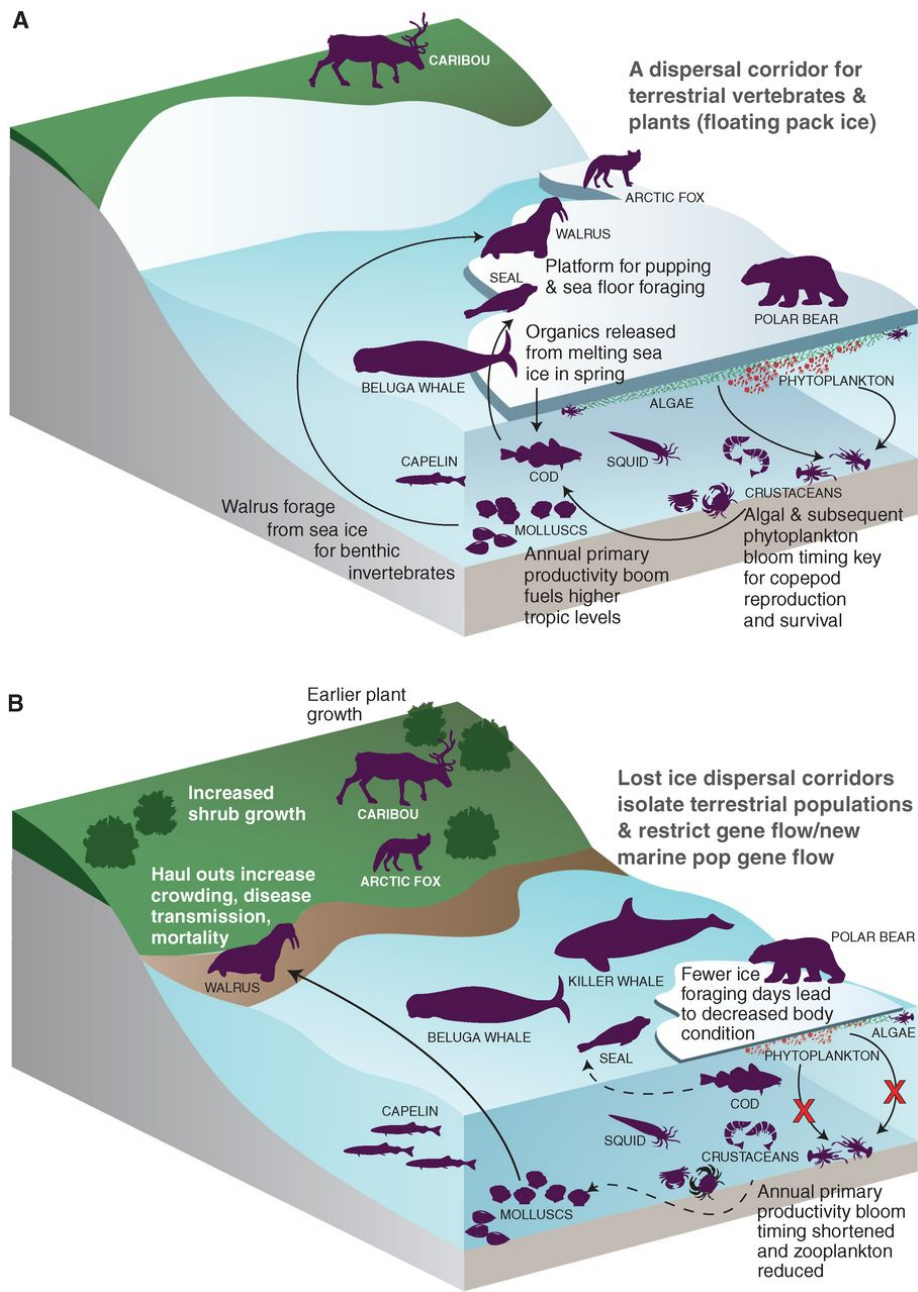


Figure 1.3: Schematic demonstrate the impacts sea ice loss impose on terrestrial and marine Arctic ecosystems. Copied from Post et al., 2013.

1.2 Sea Ice Modelling

Despite sea ice's relevance to global climate, sea ice modelling was slower to develop than other climate model components (Bitz, 2008). Early climate models incorporated sea ice by considering it as a factor of the global albedo; in this model the sea ice is functionally equivalent to a white ocean.

This fails to reflect the dynamic processes of sea ice. Sea ice varies seasonally as well as interannually, though there has been a decadal trend of sea ice loss in the Arctic (Stammerjohn, Massom, Rind, & Martinson, 2012). Unlike other glaciological responses to a warming climate, sea ice experiences no hysteresis, at least in climate models (Armour, Eisenman, Blanchard-Wrigglesworth, McCusker, & Bitz, 2011).

Advancements such as the inclusion of brine-pocket physics or the approximation of floating sea ice as viscous plastic were made possible in the 1960s and 1970s but contemporary climate models considered these elements trivial and time-consuming, leading to an era where climate models included dynamic ocean and atmosphere models but oft treated the sea ice as static and occasionally stationary (Bitz, 2008). Of the 18 modelling centers that participated in the second phase of the Coupled Model Intercomparison Project (CMIP2) in 1997, only 7 incorporated sea ice dynamics (Bitz, 2008). Later iterations of CMIP have included more complex sea ice dynamics but still lacked certain processes; ocean heat transport is known to be one of the more poorly modelled processes of sea ice in climate (Bitz, 2008). The way that the individual pieces of sea ice, called floes, disrupt and are disrupted by the surrounding thermodynamics of the ocean and atmosphere is of importance to understanding the dynamics of sea ice which is a fundamental if complex element of the global energy balance (Bitz, 2008; Horvat, Tziperman, & Campin, 2016). This work explores the thermodynamics and thermohaline impacts of sea ice in the Arctic surface ocean in hopes of providing a better idea to the overall dynamics that govern the global balance of energy.

Chapter 2

Non-Dimensional Sea Ice Counting

2.1 Heat Equation

$$\frac{\partial T}{\partial t} = \kappa \nabla^2 T + \frac{Q}{cp} \quad (2.1)$$

Where T indicates the temperature of a given fluid parcel at anytime t and at position (x, y) . $c(x, y)$ indicates the specific heat of water, which is known, as is $\rho(x, y)$, the mass density. $Q(x, y)$ indicates the heat energy spontaneously generated within the system. There are instances where Q would be greatly significant, for example heat due to solar incoming radiation or geothermal energy would be effective uses of Q . However, since this investigation focuses on the adiabatic diffusion of heat, $Q := 0$:

$$\frac{\partial T}{\partial t} = \kappa \nabla^2 T \quad (2.2)$$

The eddy diffusivity within the ocean varies across ocean basin, depth and latitude (Cole, Wortham, Kunze, & Owens, 2015). In the surface Arctic ocean, Argo float data indicates that $\kappa \in \mathcal{O}(10^2 - 10^3)$ (Cole et al., 2015).

2.2 Description of the Toy Model

A toy model was created in MATLAB and governed by the heat equation:

$$T_{i,j,t} = T_{i,j,t-1} + \frac{\kappa}{2} \left(\frac{T_{i,j-1,t-1} - T_{i,j,t-1}}{\Delta x^2} + \frac{T_{i,j+1,t-1} - T_{i,j,t-1}}{\Delta x^2} + \frac{T_{i-1,j,t-1} - T_{i,j,t-1}}{\Delta y^2} + \frac{T_{i+1,j,t-1} - T_{i,j,t-1}}{\Delta y^2} \right) \Delta t \quad (2.3)$$

where $T_{i,j,t}$ indicates the temperature of a particle located at position $x = i$, $y = j$ at time, t , diffusing relative to the diffusive constant, κ given distances Δx and Δy between $x = i$, $x = i + 1$ and $y = j$, $y = j + 1$, respectively. Periodic boundary conditions were imposed.

For each run the following values were defined as the following: $\kappa := 0.14 \frac{m^2}{s}$, $\Delta x = \Delta y = 1 m$, and $\Delta t = 1 s$.

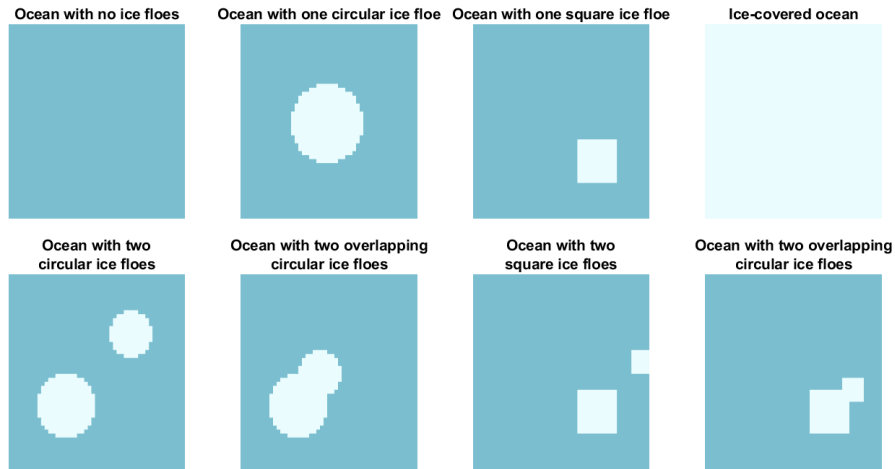


Figure 2.1: An example of different potential ice floe distributions described by the language that is used within this paper².

To compare the diffusion across a variety of ice floes, binary images were created to signify a region of ice that was inhabited by both ice and ocean, using a combination of randomized and intentionally chosen geometries.

In this visualization of some ice floe geometries, white blocks indicate a ice-filled region and blue represents the ice-free ocean (Fig. 2.1). While the initial conditions are binary, the intermediate temperature states are not, as shown in Fig 2.2.

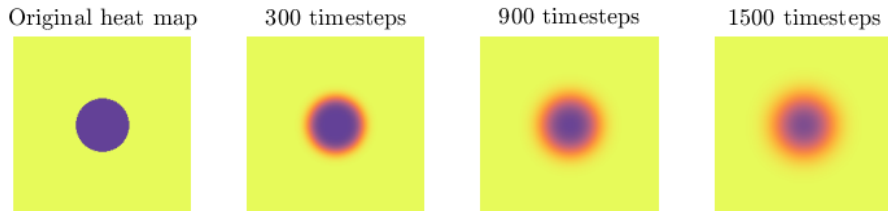


Figure 2.2: Illustration of diffusive heat transference over time in the MATLAB Toy Model. The example used is a 200 m by 200 m ocean with a circular ice floe of radius 30 m centered in the middle. Each timestep indicates a second.

²The colorscheme of these and all other ice geometry maps is enabled by the creators of cmocean: Kristen M. Thyng, Chad A. Greene, Robert D. Hetland, Heather M. Zimmerle, and Steven F. DiMarco.

2.3 Central Ice Floes of Increasing Diameter

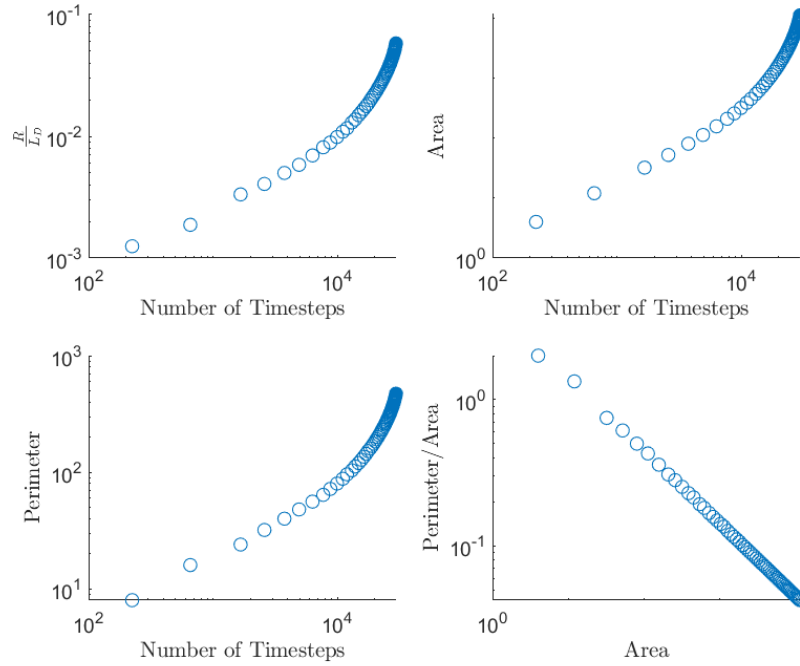


Figure 2.3: The number of timesteps (seconds) needed to complete 3 e-folds of variance for a 100 m by 100 m ocean with central ice floe with radii ranging from 1 m to 50 m.

When just the ice floe distribution was limited to just one ice floor located in the center of the ocean, the the number of timesteps needed to diffuse the heat increase exponentially with the area, perimeter and the ratio of the area to perimeter (Fig. 2.3).

2.4 An example of an ocean with 10 circular ice floes of pre-determined radii

It was hypothesized that the number of timesteps required to homogenize the temperature beneath a specific ice floe geometry was strongly correlated to the ratio of the area and the perimeter. To explore this hypothesis, 300 ice floe geometries were generated using a specific set of radii (four circles of radius 4 m, two circles of radius 3 m, two circles of radius 4 m and two circles of radius 6 m) in an otherwise identical 100 m by 100 m ocean. Twelve of these pseudo-randomized floes are visualized in Fig. 2.4.

When tested, this set of ice floe distributions did support this hypothesis, but only weakly as similar ratio of area to perimeter sometimes corresponded to ice floe distributions that required vastly differing times to equilibrate the heat (Fig. 2.5).

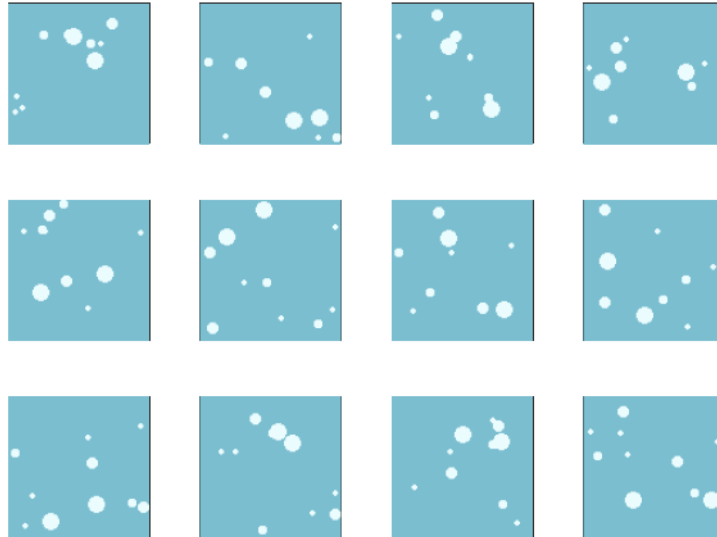


Figure 2.4: 12 examples of the 300 random ice floe geometries studied in this section. The distribution of radii are as follows: four circles of radius 4 m, two circles of radius 3 m, two circles of radius 4 m and two circles of radius six m. The overall ocean dimension is 100 m by 100 m.

This lack of a correlated relationship persisted regardless of the amount of overlap of the ice floes (Fig. 2.5). In Figure 2.5, the yellow markers indicate floes with minimal (less than sixteen m^2) of overlapping ice floe, whereas red indicates moderate (more than sixteen m^2 but less than 45 m^2) of overlapping ice floe and blue indicates severe ice floe overlapping; any configuration with more than 45 overlapping ice m^2 floe grid points.

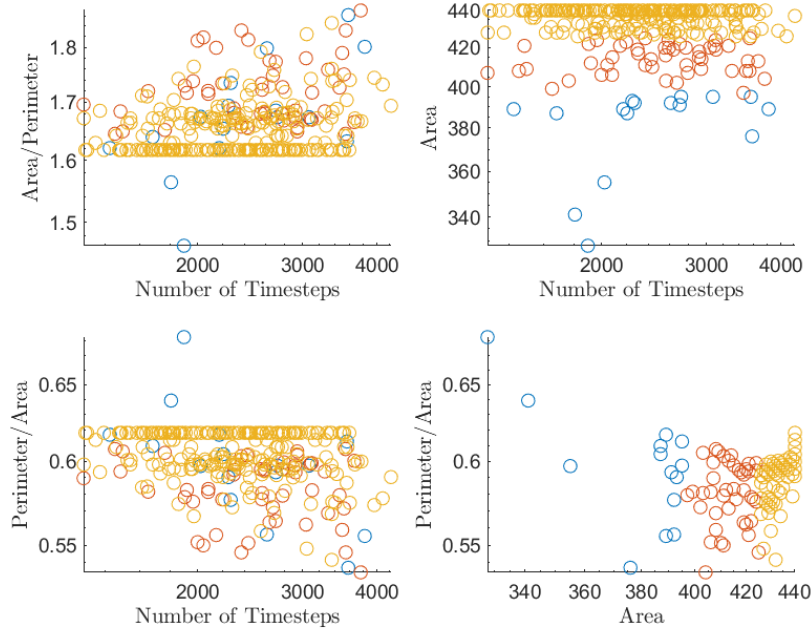


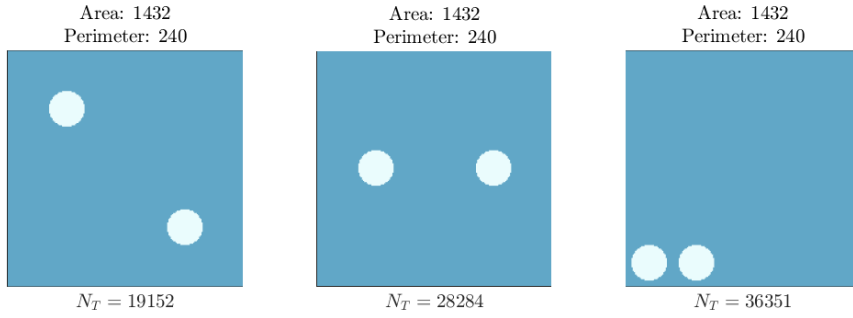
Figure 2.5: Relationship of area, perimeter and number of time steps to achieve 3 e-folds of the variance for 300 pseudo-randomized sea ice floe distributions. Distributions were composed of ten circles with radii 2, 2, 4, 4, 6, 6, 2, 2, 3 and 3 m in a 100 m by 100 m ocean.

While the ratios of perimeter to area were relatively constant the number of timesteps needed to homogenize the ocean varied greatly. A Spearman coefficient of correlation indicates that there is only a weak ($r = 0.2909$) correlation though the low p-value ($p = 2.9 \times 10^{-7}$) indicates that this is a statistically significant result.

Conversely there was a far stronger statistically-significant relationship, ($r = 0.5719$, $p = 1.8 \times 10^{-29}$) between the spatial organization of the ice floes and the number of timesteps needed to complete the e-folding. To calculate the correlation of this relationship, the variation in spatial organization was assessed by determining the standard deviation of each quartile of the ocean and then determining the standard deviation amongst the four quartiles. The two methods are compared and contrasted on the following page.

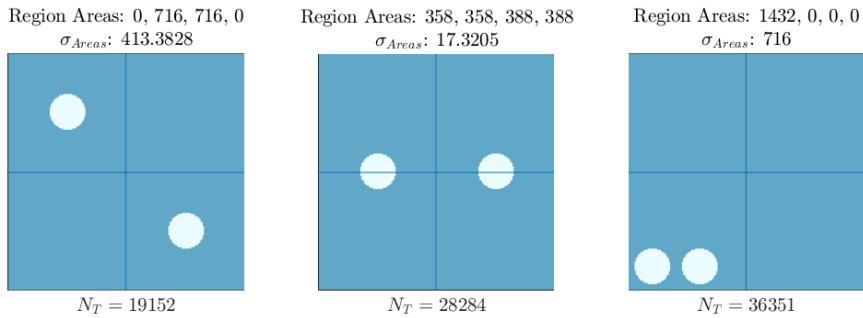
Area-Perimeter Method

This algorithm calculates the total area of ice-encased ocean and compares it to the perimeter of the ice floes. While the exact estimate of required timesteps to homogenize heat, N_T depends on κ , a rough estimate can be gleaned just from this ratio. However, while this method appropriately models single floe diffusive properties, it is less effective at predicting complex ice floe distributions. Fig. 2.4 illustrates how a number of ice floes with identical area-to-perimeter ratios vary in time steps required to homogenize.



Interquartile Method

This algorithm divides the ocean into a number of regions (namely four) and calculates the standard deviation of these regions. Because the ocean is periodic, the dividing lines for the ocean were arbitrarily chosen along the meridians below (Fig. 2.4). While the choice was made out of computational convenience, the position of these boundaries does absolutely impact the interregional variance in area and so the algorithm could be improved to optimize the functionality at the expense of immediacy. These cases indicate that there is residual resolution sensitivity in the approach so the current scaling laws are not scale-aware.



When this sample dataset was analyzed to find the optimal number of regions to divide an “ocean” into, the 3x3 was shown to have the highest correlation between interregional standard deviation and number of timesteps required to homogenize the temperature and the 2x2 was shown to be only marginally worse.

n-th root of number of regions	correlation
2	0.5719
3	0.5817
4	0.4455
5	0.3912
6	0.2424
7	0.2728
8	0.1288
9	0.2982
10	0.2338

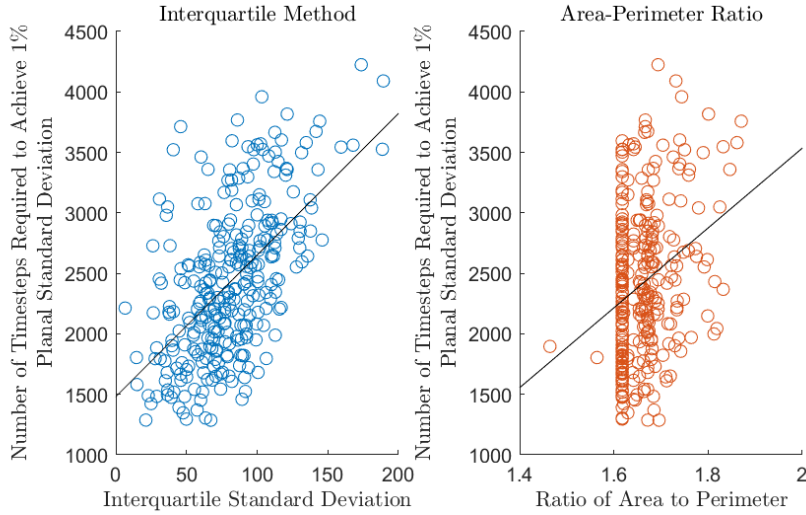


Figure 2.6: Comparison of the interquartile method and the area-perimeter method to calculate the number of timesteps needed for diffusion, over the case of four randomly constructed radii.

The relationship predicted by the least-squares regression line is below (Eq. 2.4). Notably, the fit does not behave as well for some more easily diffused initial conditions.

$$N_T \approx 12 q_{std} + 15,000 \quad (2.4)$$

2.5 An example of an ocean with 4 circular ice floes of randomized radii

To analyze if the internal geometry or spatial geometry dominated other floe formations, these correlations were compared across various distribution of radii. One such ensemble was created by running simulations with four circles of random-length radii, $r_n = x \mid 1 \leq n \leq 4, 1 \leq x \leq 10$.



Figure 2.7: Four examples of the 300 random ice floe geometries studied in this section. The distribution of radii are randomized within the range of whole numbers between one and ten inclusive.

For this dataset, the original hypothesis faired better; Spearman's coefficient of correlation was 0.7394. Here still, the interquartile method was equally effective and produced a correlation of 7.420. Both methods resulted in a p-value, $p < 10^{-52}$.

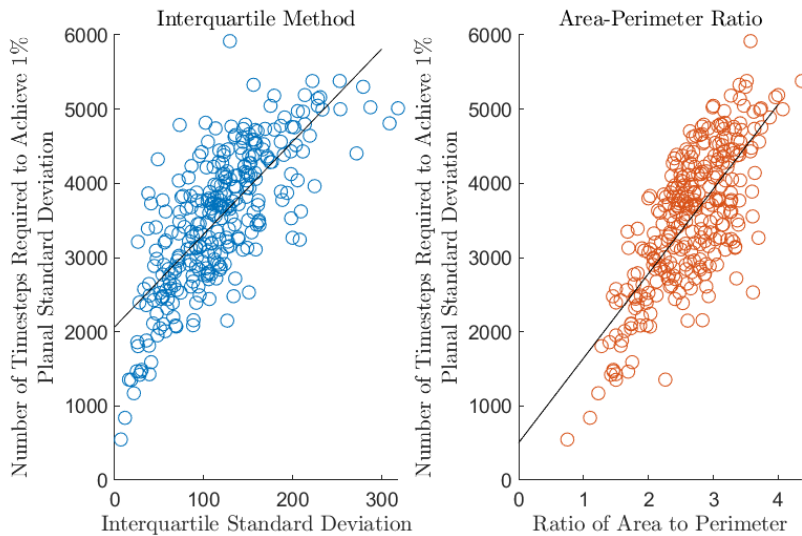


Figure 2.8: Comparison of the interquartile method and the area-perimeter method to calculate the number of timesteps needed for diffusion, over the case of four randomly constructed radii.

Utilizing the MITgcm

3.1 Description of the Model

The MITgcm is a non-hydrostatic general circulation model encoded with salinity, temperature and density, among many other variables, that has seen regular modification since its creation in 1995 (Adcroft et al., 2008). For this study a 10 km by km ocean was modelled with polar geophysical constants, such as a high-latitude Coriolis force, cool average ocean temperature and low salinity.

3.2 Idealized One-Dimensional Floes

A series of circular floes were examined using the mechanics of the MITgcm (Fig. 3.1). The floes depicted in Fig. 3.1 each represent an ice floe with radii less than the Rossby Deformation Radius of the Deep Arctic Ocean, however the larger floes would exceed the empirical Rossby Radius near the continental shelves (Nurser & Bacon, 2014).

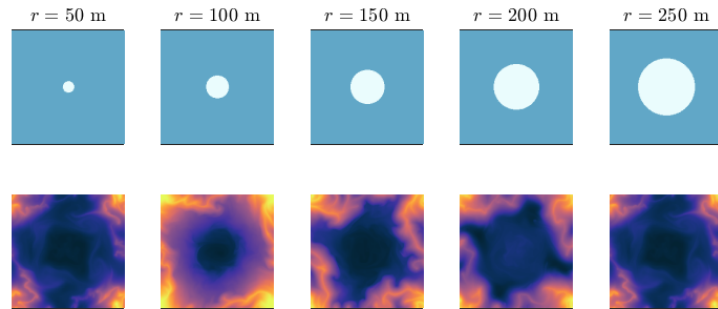


Figure 3.1: *Top Row*: Initial ice floe distributions in a 10 km by 10 km ocean. *Bottom Row*: Final heat distribution after 1,276 hours of simulated heat flow.

The distribution of how heat and salinity varied in the surface ocean for a specific run ($r = 150$ m) are explored in further detail in Figs. 3.2 and 3.3. The vertical velocity and directionality of the surface water at these same time intervals can be seen in Fig. 3.4.

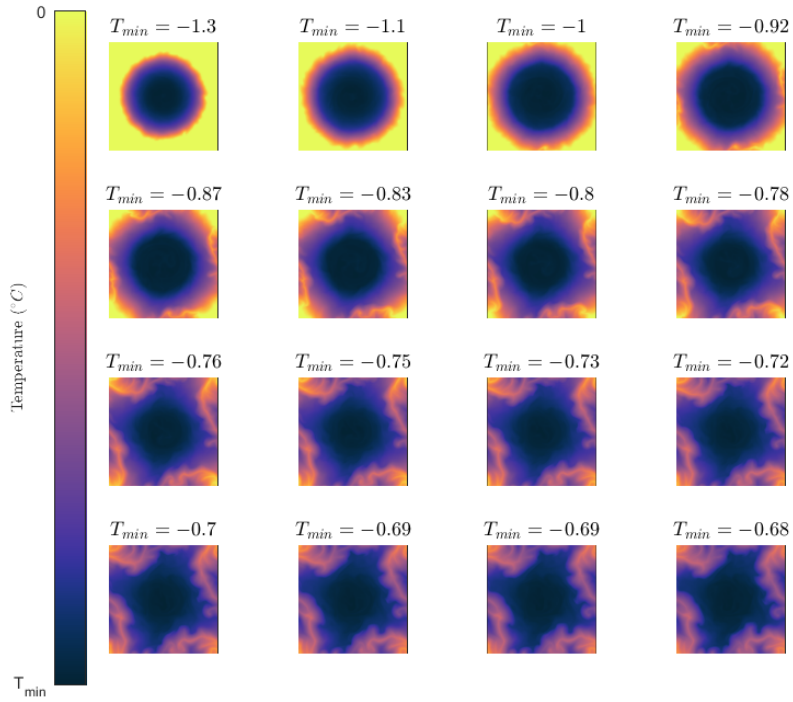


Figure 3.2: Thermal evolution of surface ocean heat distribution provided one circular floe from 4 to 1,276 hours into dispersion. Read left to right, and top to bottom.

Unlike the purely diffusive MATLAB model, the MITgcm transfers heat through eddy dynamics as can be seen in the evolution of heat and salinity distribution within a timeseries (Figs. 3.2 and 3.3). This is consistent with previous models of sub-floe ocean mechanics (Horvat et al., 2016).

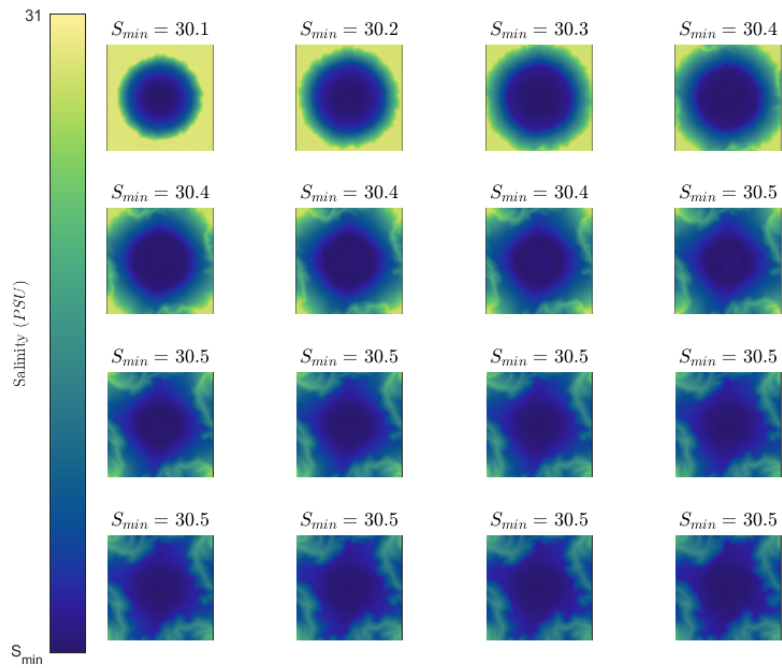


Figure 3.3: Evolution of surface ocean salinity distribution provided one circular floe from 4 to 1,276 hours into dispersion. Read left to right, and top to bottom.

In both the surface ocean salinity and temperature plots, the range of surface values changed significantly throughout the timeseries; in both cases the range of values was almost halved. While this indicates that the surface ocean was becoming more homogenized, irregularities still persisted specifically along eddy currents.

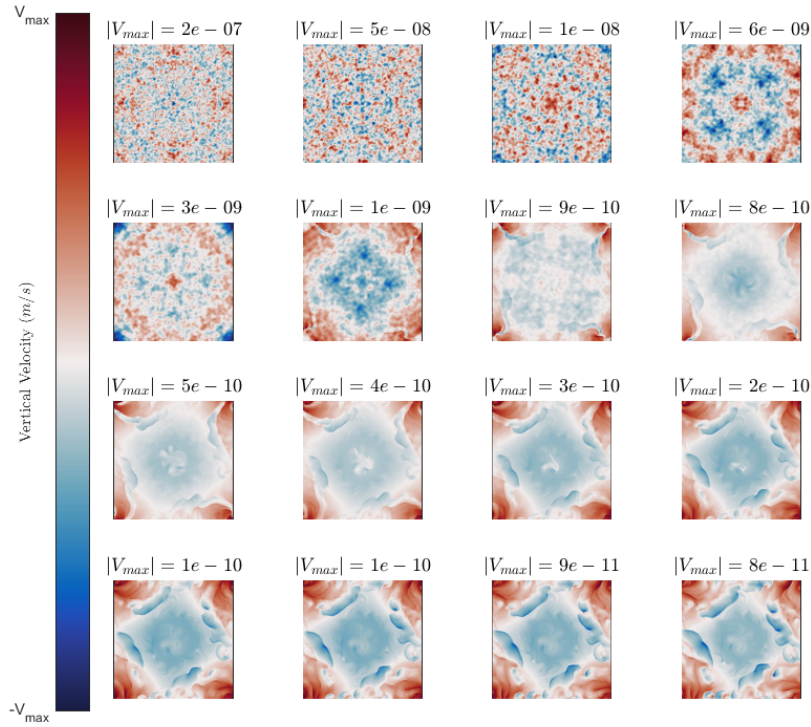


Figure 3.4: Evolution of surface ocean vertical velocity distribution provided one circular floe from 4 to 1,276 hours into dispersion. Read left to right, and top to bottom.

Figure 3.4 indicates the evolution of the regions of upwelling and downwelling of the surface ocean around the floe. Within the first days of destabilizing the surface ocean, small eddies form with high velocities, however after reaching some stability the eddy forms into a more consistent cycle that downwells under the ice floe and upwells in the corners, which represent the ocean farthest from the initial ice floe (Fig. 3.4). The initial vertical velocity is three orders of magnitude greater than the later values indicating how significantly the overturning decreases as the ocean has time to approach hydrostatic balance 3.4. Further illustration of the eddy velocity dynamics over time is available in the appendix, including plots of zonal and meridional velocity as well as vertical, zonal and meridional velocity at a variety of ocean cross-sections.

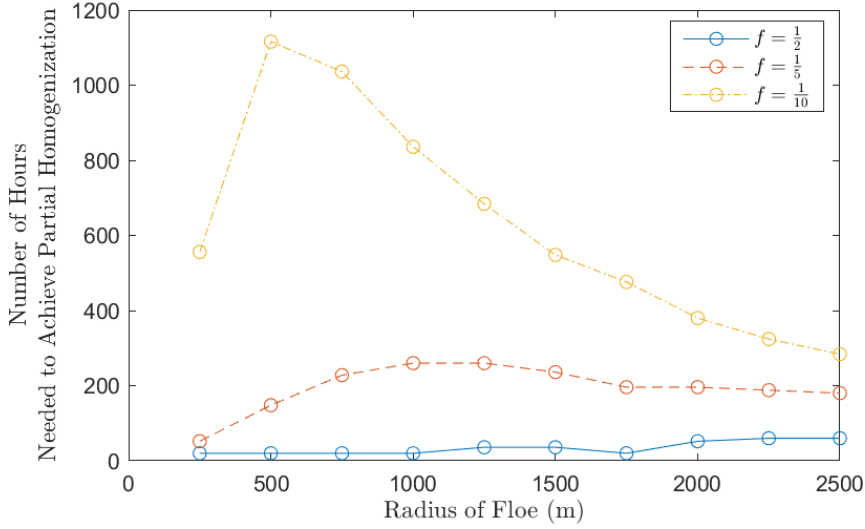


Figure 3.5: The number of hours needed within the MITgcm simulation after which the standard deviation of the ocean’s temperature was equal to $f\sigma_0$ as a function of f and the radius of the initial ice floe in the 10 km by 10 km ocean.

Because the MITgcm was more computationally expensive than the purely diffusive model, it was not practical to allow the model to run until three e-folds of the standard deviation had transpired. For that reason, simpler comparisons were made (Fig. 3.5).

The standard deviation of the surface ocean was found at the initial condition, vertically-averaged over the upper 12.5 m (σ_0). The time (measured in 8 hour increments) until the standard deviation of the ocean, σ was less than $f \cdot \sigma_0$ was recorded for each of a number of MITgcms differing only in the radius of the individual floe. As can be seen in Fig. 3.5, the radius of the ice floe for which the peak number of timesteps decreases with f . At least within these data points, the relationship between the number of timesteps needed to partially homogenize a ocean (with $f < \frac{1}{10}$) and the radius of the floe is opposite in the MITgcm compared to the purely diffusive model, a function of the heat transport mechanics of eddies. This indicates that κ_{MITgcm} is not constant across floe dimension.

3.3 More Complex Geometries

A number of more complex floe patterns were evaluated using the MITgcm. The initial ice distribution and final heat distribution are illustrated in Fig. 3.6.

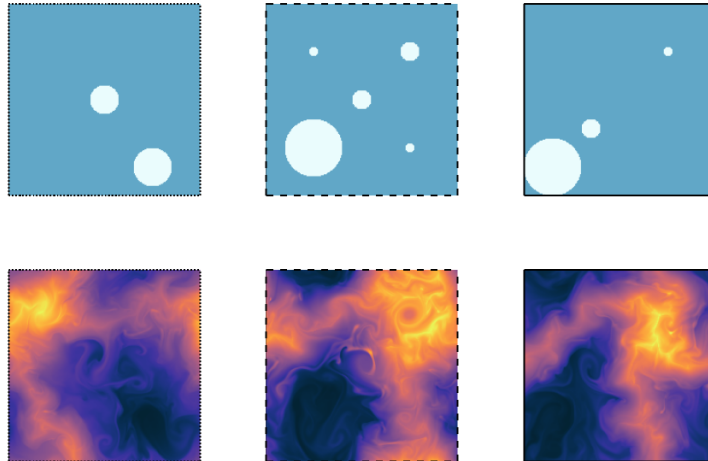


Figure 3.6: *Top Row*: Initial ice floe distributions in a 10 km by 10 km ocean. *Bottom Row*: Final heat distribution after 1,276 hours of simulated heat flow. The outlines identify the separate runs in Fig. 3.12.

The evolution of heat, salinity and vertical velocity for the ocean with initial ice floes is displayed in the next three pages. While the specifics vary due to the more complex floes, the underlying range and mechanism of salinity, heat and overturning circulation remain the same between the model runs with singular floes and the model run with two floes (Figs. 3.2, 3.3, 3.4, 3.7, 3.8 and 3.9).

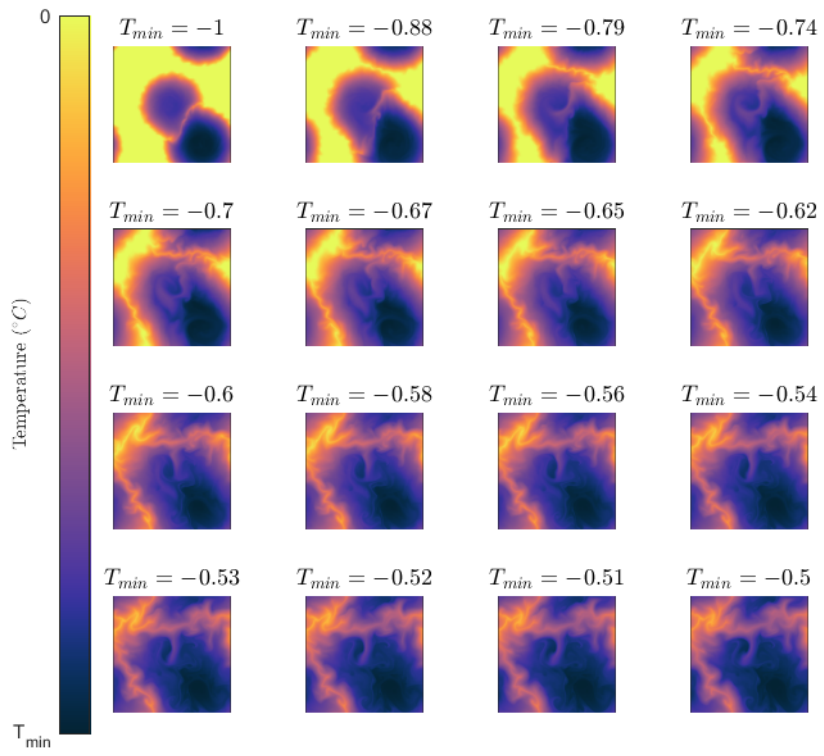


Figure 3.7: Thermal evolution of an ocean provided two circular floes from 4 to 1,276 hours into dispersion. Read left to right, and top to bottom.

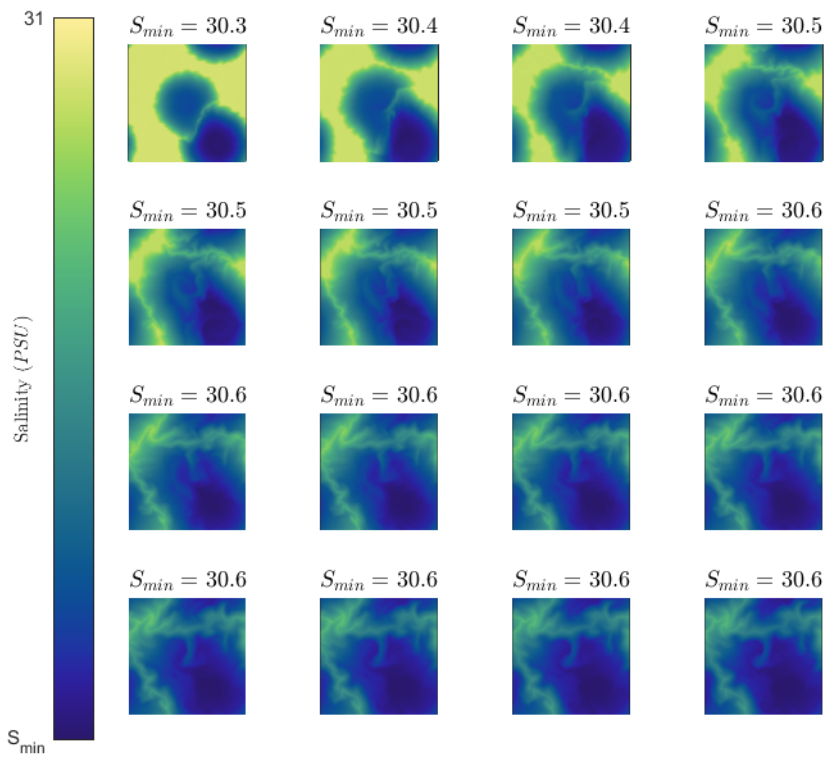


Figure 3.8: Salinity evolution of an ocean provided two circular floes from 4 to 1,276 hours into dispersion. Read left to right, and top to bottom.

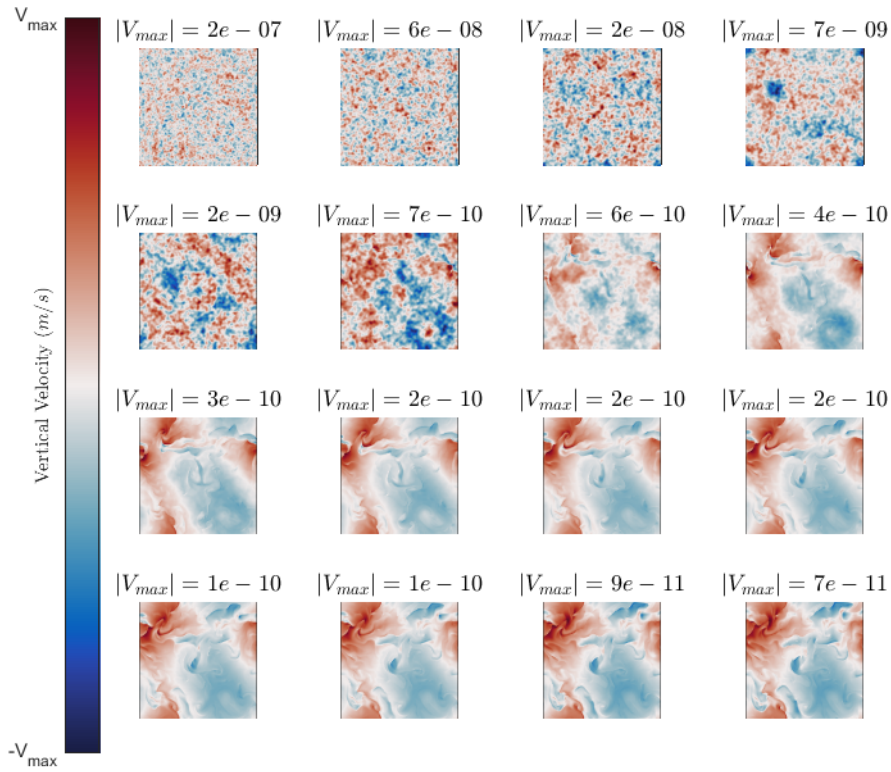


Figure 3.9: Vertical velocity evolution of an ocean provided two circular floes from 4 to 1,276 hours into dispersion. Read left to right, and top to bottom.

3.4 Comparing the Toy Model and the MITgcm

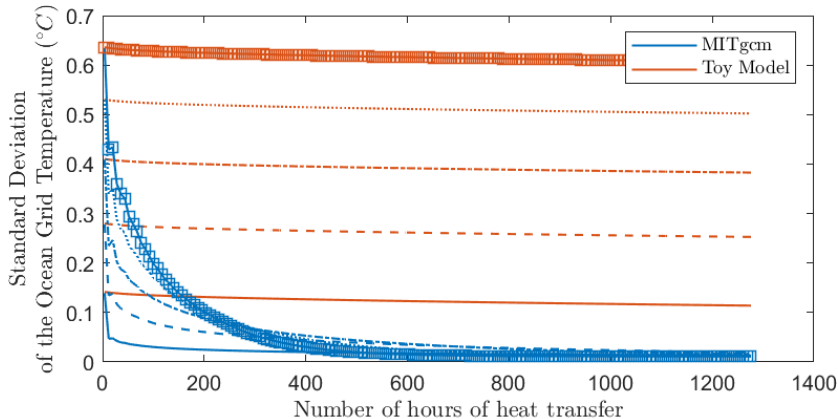


Figure 3.10: A comparison³ of change in standard deviation over time when modelled by the toy model with $\kappa = 1.4 \times 10^{-7} \frac{m^2}{s}$ (red) and MITgcm (blue). For both scenarios, the initial condition was a circular ice floe of radii 500, 1000, 1500, 2000 and 2500 m centered in a 10 km by 10 km otherwise ice-less ocean.

The MITgcm model is poorly modelled by the purely diffusive model when $\kappa := 1.4 \times 10^{-7} \frac{m^2}{s}$, the constant of thermal diffusivity of water molecularly (Fig. 3.10). The MITgcm is far better modelled when $\kappa = 1.7 \times 10^3 \frac{m^2}{s}$, though this relation too is problematized (Fig. 3.11). For each of the five runs there exists at least one point x_* wherein preceding timesteps the Toy Model calculates less diffusion than the MITgcm and for the following timesteps the Toy Model overcalculates the diffusivity of the MITgcm (Fig. 3.11). Therefore it can be assumed that $\kappa_{MITgcm} = f(\sigma)$, where σ is the standard deviation of the ocean temperature.

For a few cases, the variance within the MITgcm decreased before increasing again. This is due to the heat transport mechanisms of eddies which can redistribute heat in such a way that it concentrates warmth as much as disperses it. As one would expect, the purely diffusive model is monotonically decreasing. The evolution of heat over time in the MATLAB model can be seen in Fig. 2.2.

³Because the MITgcm is a three-dimensional model instead of a two-dimensional model, the standard deviation of the ocean was assessed by finding the vertical average of the first five grid points approximating the highest 12.5 m of ocean. A justification is presented in Fig. 3.13.

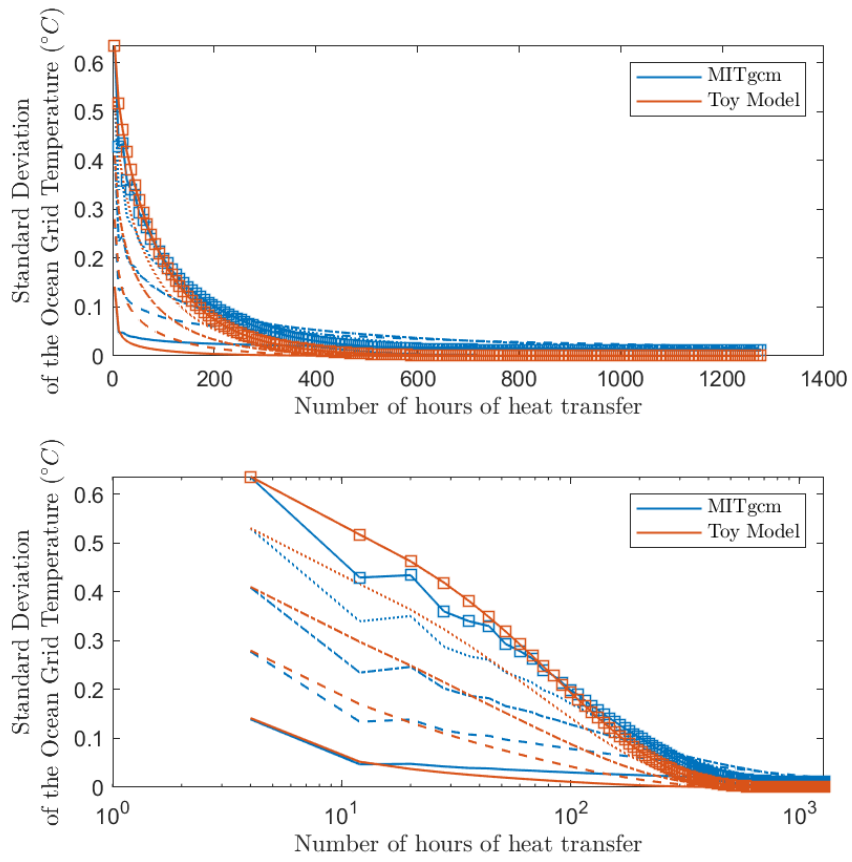


Figure 3.11: A comparison of change in standard deviation over time when modelled by the toy model with $\kappa = 1.7 \times 10^3 \frac{m^2}{s}$ (red) and MITgcm (blue) with the same initial conditions as Fig. 3.10.

Using the Diffusive Model to Approximate More Complex Floes

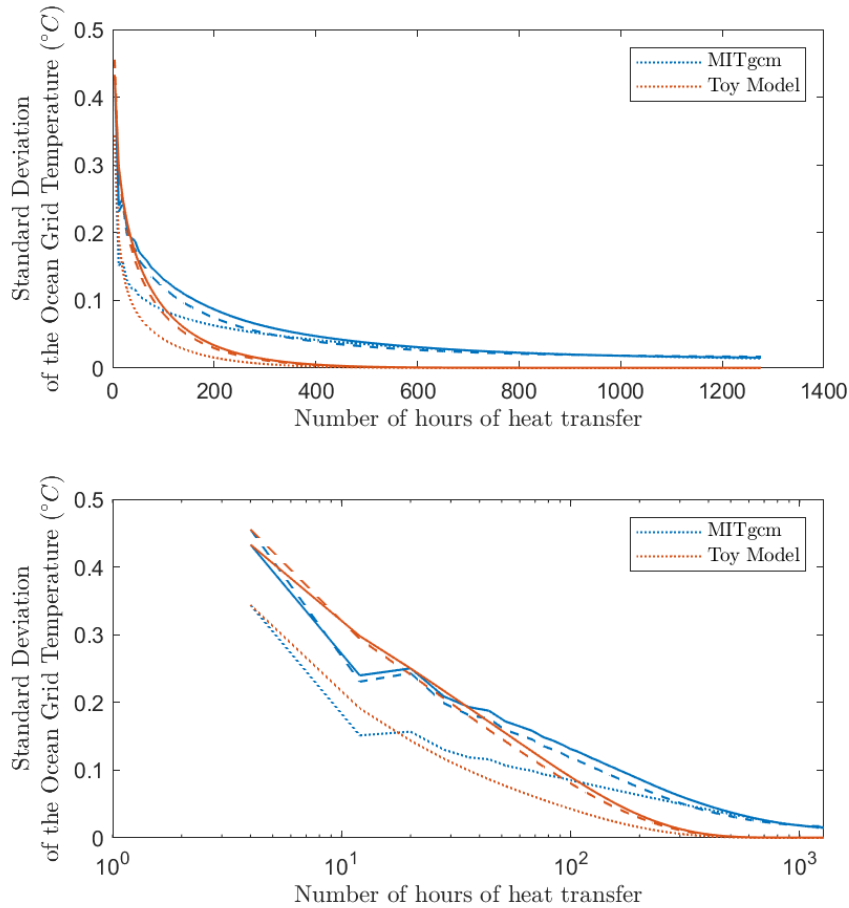


Figure 3.12: A comparison of change in standard deviation over time when modelled by the toy model with $\kappa = 1.7 \times 10^3 \frac{m^2}{s}$ (red) and MITgcm (blue) given the complex floe geometry described in Chapter 3.

In following with the analysis on the previous pages, the more complex run used to compare the MITgcm and the Toy Model. The Toy Model was only marginally less effective at modelling the rate of homogenization with two floes than with one. Similarly to the singular floe examples, the purely diffusive toy model first underestimates and then overestimates κ_{MITgcm} , leading to a somewhat inaccurate prediction. The diffusive model is overall less reflective of the MITgcm during these more complex floes, further indicating that κ_{MITgcm} is a function of the floe distribution.

Deciding the Analysis Depth

To compare the MITgcm and the MATLAB model, it was important to decide what region of the MITgcm to analyse. The upper ocean was the most dynamic, but heat was not conserved as cool and warm water would attempt hydrostatic balance by concentrating the warm water at the surface (Fig. 3.13). Lower ocean waters, however, are only weakly constrained by the ice floe and have a original heat signature variant from the MATLAB model. For that reason it was chosen to analyze a vertical average of a set number of grid cells, which each signify 2.5 m of ocean water. The average of the first five grid points, indicating a depth of 12.5 m best conserved energy and matched the total heat distribution of the MATLAB simulation (Fig. 3.13).

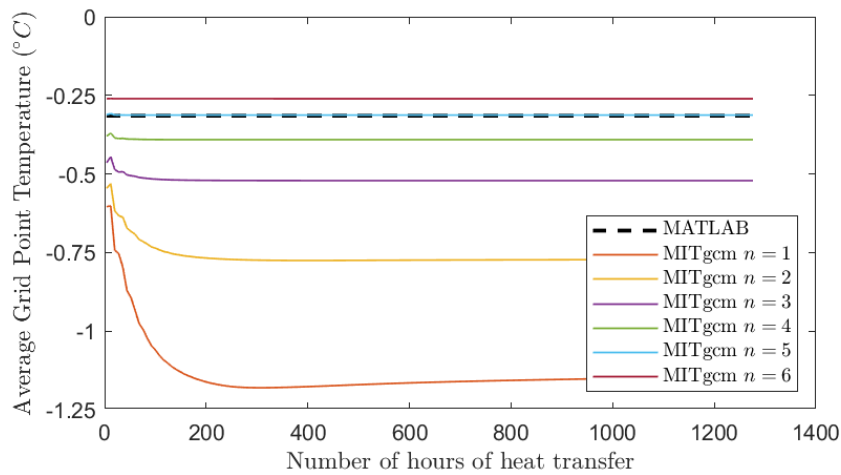


Figure 3.13: A comparison of the MATLAB model and the mixed layer depths of the ocean. The MATLAB model most closely follows the average of the first five grid cells indicating a depth of 12.5 m of the ocean.

Chapter 4

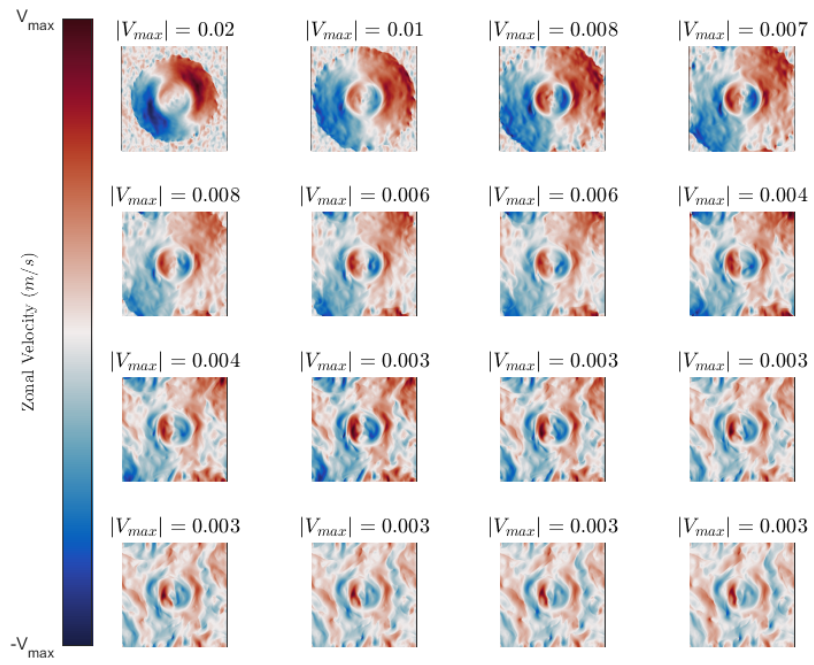
Conclusions

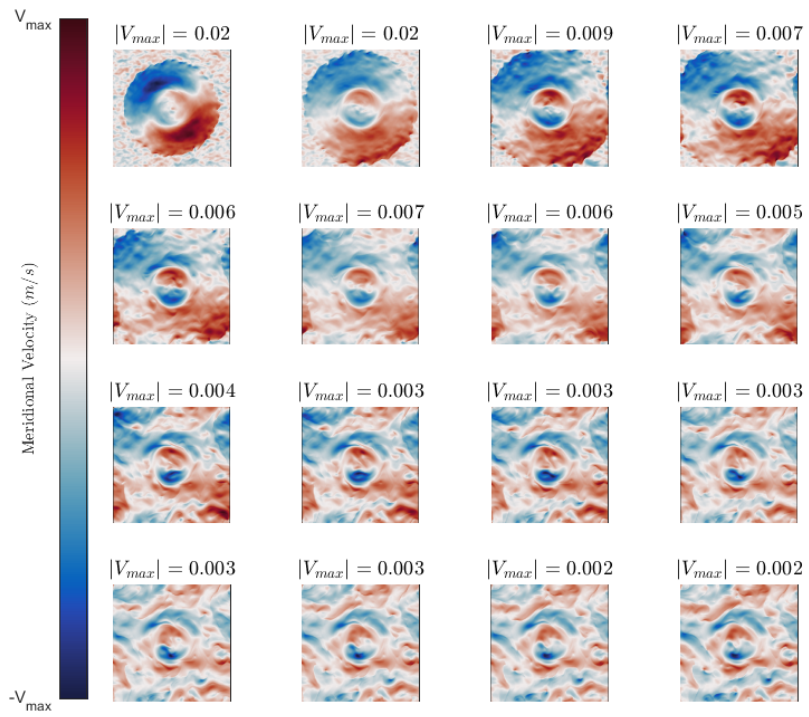
The hydrostatic instabilities of sea ice formation create localized eddies that redistribute heat and salinity within the surface ocean. The horizontal eddy diffusivity, κ of the MITgcm was found to be a non-monotonic function of the heat distribution of the ocean. According to previous studies by Cole et al., $\kappa \in \mathcal{O}(10^3)$ is a relatively realistic parameter for surface ocean eddy diffusivity in the polar ocean.

The magnitude of the eddy vorticity decreases with time however these eddies persist for at least 1,200 hours. While these eddies cannot be modelled in a purely diffusive toy model the rate of heat distribution, κ , and total time required to homogenize an ocean region, T_H , can be. Moreover the diffusive model can be roughly approximated by examining the initial conditions of the ocean if sufficient similar geometries have been examined previously.

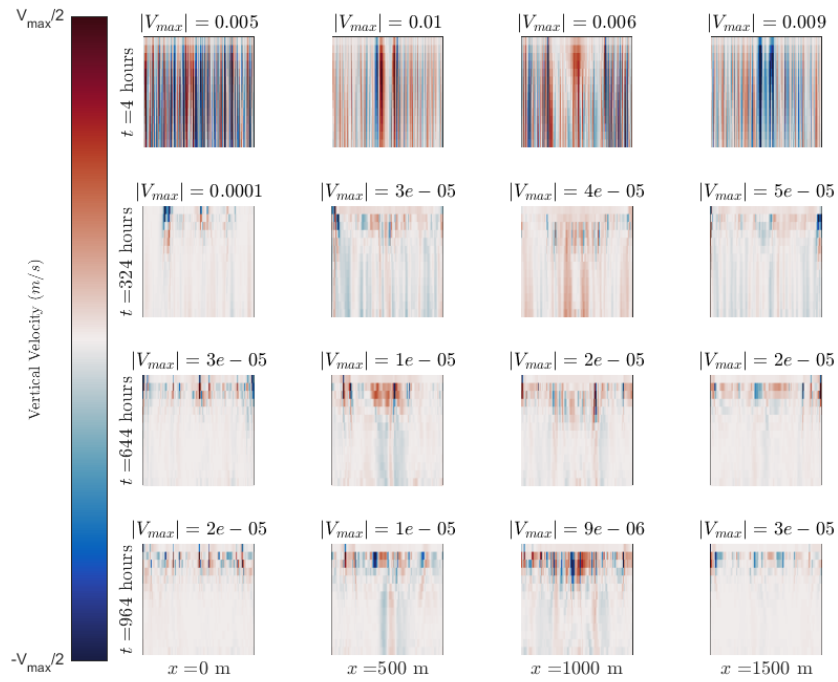
Appendix

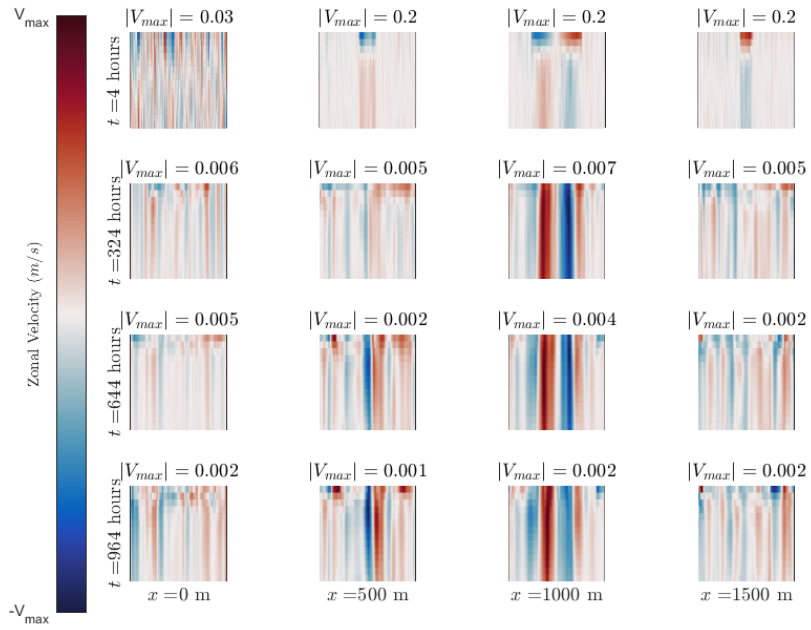
Meridional and zonal velocity plots of the surface ocean

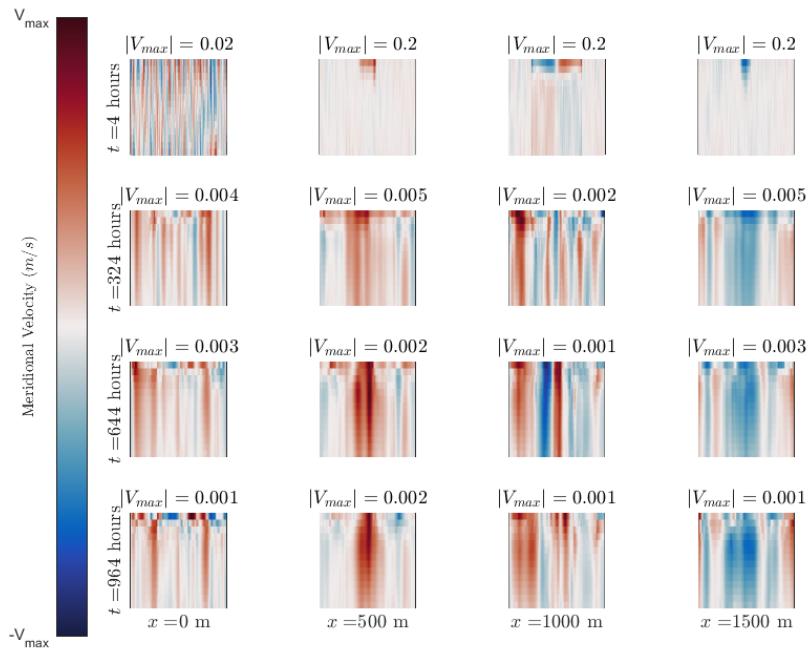




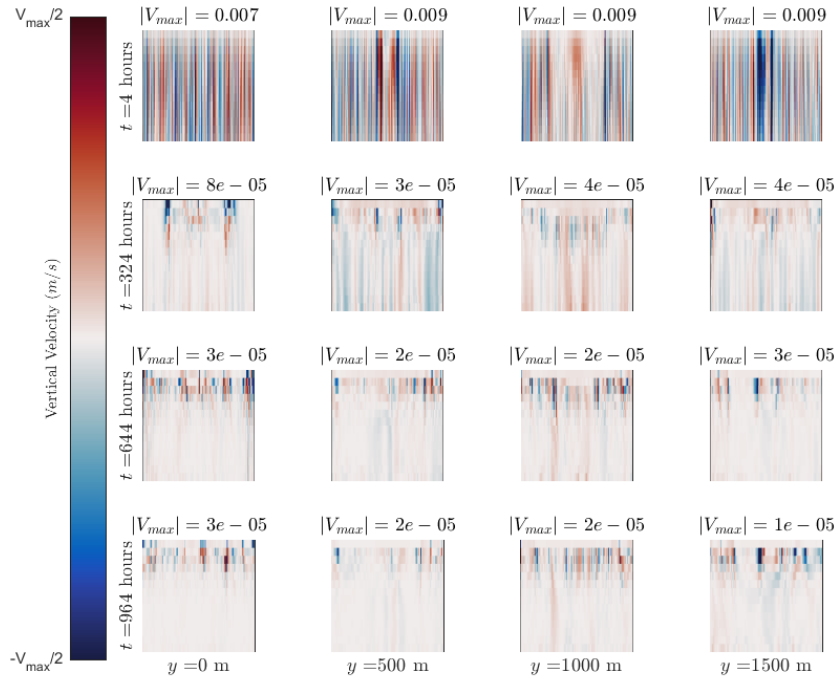
Zonal cross-sections of vertical, zonal and meridional velocity timeseries

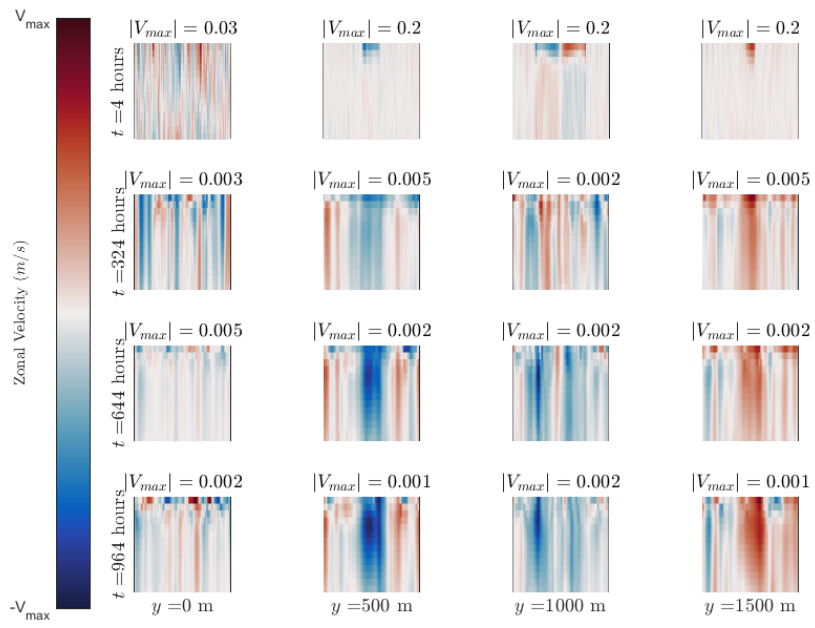


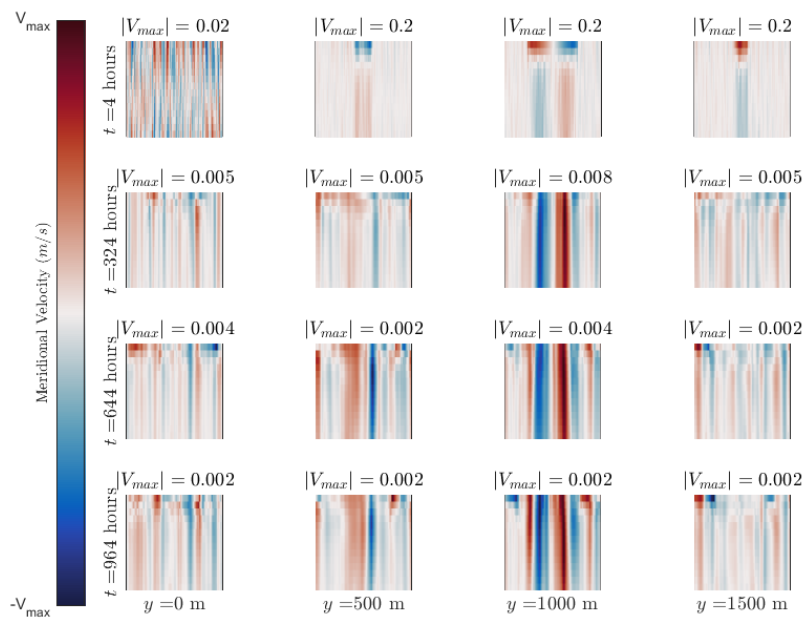




Meridional cross-sections of vertical, zonal and meridional velocity timeseries







Acknowledgments

There are a number of people without whom I'd not be a geophysics student, not to mention finishing this senior thesis. The first acknowledgment must go to Baylor Fox-Kemper who recognized something in me before I ever did and has graced my last three years at Brown with his knowledge, support and wonderful sense of humor. A number of other professors have supported me; Will Hicks, Jung-Eun Lee and Meredith Hastings stand out, and I am deeply grateful to all. Thanks too goes to the graduate students who encouraged me, the undergrads who commiserated with me and the family that loved me so much they edited this same thesis three different times at various state of completion.

References

- Adcroft, A., Campin, J., Dutkiewicz, S., Evangelinos, C., Ferreira, D., Forget, G., ... others (2008). *Mitgcm user manual*. MIT Department of EAPS Cambridge.
- Armour, K., Eisenman, I., Blanchard-Wrigglesworth, E., McCusker, K., & Bitz, C. (2011). The reversibility of sea ice loss in a state-of-the-art climate model. *Geophysical Research Letters*, *38*(16).
- Backus, G. A., & Strickland, J. H. (2008). *Climate-derived tensions in arctic security*. (Tech. Rep.). Sandia National Laboratories.
- Berkes, F., & Jolly, D. (2002). Adapting to climate change: social-ecological resilience in a canadian western arctic community. *Conservation ecology*, *5*(2), 18.
- Bitz, C. M. (2008). *Numerical modeling of sea ice in the climate system*. Tech. Rep., University of Washington, available at: www.atmos.uw.edu.
- Boetius, A., Anesio, A. M., Deming, J. W., Mikucki, J. A., & Rapp, J. Z. (2015). Microbial ecology of the cryosphere: sea ice and glacial habitats. *Nature Reviews Microbiology*, *13*(11), 677.
- Born, A., Nisancioglu, K. H., & Risebrobakken, B. (2011). Late eemian warming in the nordic seas as seen in proxy data and climate models. *Paleoceanography*, *26*(2).
- Cole, S. T., Wortham, C., Kunze, E., & Owens, W. B. (2015). Eddy stirring and horizontal diffusivity from argo float observations: Geographic and depth variability. *Geophysical Research Letters*, *42*(10), 3989–3997.
- Comfort, G., Dinovitzer, A., Lazor, R., & Hinnah, D. (2004). Offshore arctic pipeline oil spill risk assessment. In *2004 international pipeline conference* (pp. 2535–2542).
- Cunningham, S., Baringer, M., Johns, B., Toole, J., Osterhaus, S., Fischer, J., ... others (2010). The present and future system for measuring the atlantic meridional overturning circulation and heat transport. OceanObs'09.
- Curry, J. A., Schramm, J. L., & Ebert, E. E. (1995). Sea ice-albedo climate feedback mechanism. *Journal of Climate*, *8*(2), 240–247.
- Derocher, A. E., Lunn, N. J., & Stirling, I. (2004). Polar bears in a warming climate. *Integrative and comparative biology*, *44*(2), 163–176.
- de Vernal, A., Gersonde, R., Goosse, H., Seidenkrantz, M.-S., & Wolff, E. W. (2013). Sea ice in the paleoclimate system: the challenge of reconstructing sea ice from proxies—an introduction. *Quaternary Science Reviews*, *79*, 1–8.
- Dodds, K. (2008). *Icy geopolitics*. SAGE Publications Sage UK: London, England.

- Dokken, T. M., Nisancioglu, K. H., Li, C., Battisti, D. S., & Kissel, C. (2013). Dansgaard-oeschger cycles: Interactions between ocean and sea ice intrinsic to the nordic seas. *Paleoceanography and Paleoclimatology*, *28*(3), 491–502.
- Ebinger, C. K., & Zambetakis, E. (2009). The geopolitics of arctic melt. *International Affairs*, *85*(6), 1215–1232.
- Ferrari, R., Jansen, M. F., Adkins, J. F., Burke, A., Stewart, A. L., & Thompson, A. F. (2014). Antarctic sea ice control on ocean circulation in present and glacial climates. *Proceedings of the National Academy of Sciences*, *111*(24), 8753–8758.
- Gautier, D. L., Bird, K. J., Charpentier, R. R., Grantz, A., Houseknecht, D. W., Klett, T. R., . . . others (2009). Assessment of undiscovered oil and gas in the arctic. *Science*, *324*(5931), 1175–1179.
- Goosse, H., & Fichefet, T. (1999). Importance of ice-ocean interactions for the global ocean circulation: A model study. *Journal of Geophysical Research: Oceans*, *104*(C10), 23337–23355.
- Gosselin, M., Levasseur, M., Wheeler, P. A., Horner, R. A., & Booth, B. C. (1997). New measurements of phytoplankton and ice algal production in the arctic ocean. *Deep Sea Research Part II: Topical Studies in Oceanography*, *44*(8), 1623–1644.
- Horvat, C., Tziperman, E., & Campin, J.-M. (2016). Interaction of sea ice floe size, ocean eddies, and sea ice melting. *Geophysical Research Letters*, *43*(15), 8083–8090.
- Humpert, M., & Raspotnik, A. (2012). The future of arctic shipping along the transpolar sea route. *Arctic Yearbook*, *2012*(1), 281–307.
- Lemelin, R. H. (2006). The gawk, the glance, and the gaze: Ocular consumption and polar bear tourism in churchill, manitoba, canada. *Current Issues in Tourism*, *9*(6), 516–534.
- Ludescher, J., Yuan, N., & Bunde, A. (2018). Detecting the statistical significance of the trends in the antarctic sea ice extent: an indication for a turning point. *Climate Dynamics*, 1–8.
- Marshall, J., & Speer, K. (2012). Closure of the meridional overturning circulation through southern ocean upwelling. *Nature Geoscience*, *5*(3), 171.
- Nicholls, R. J., Marinova, N., Lowe, J. A., Brown, S., Vellinga, P., De Gusmao, D., . . . Tol, R. S. (2011). Sea-level rise and its possible impacts given a beyond 4 c world in the twenty-first century. *Philosophical Transactions of the Royal Society A: Mathematical, Physical and Engineering Sciences*, *369*(1934), 161–181.
- Nurser, A., & Bacon, S. (2014). The rossby radius in the arctic ocean. *Ocean Science*, *10*(6), 967–975.
- Pohlmann, H., Sienz, F., & Latif, M. (2006). Influence of the multidecadal atlantic meridional overturning circulation variability on european climate. *Journal of climate*, *19*(23), 6062–6067.
- Post, E., Bhatt, U. S., Bitz, C. M., Brodie, J. F., Fulton, T. L., Hebblewhite, M., . . . Walker, D. A. (2013). Ecological consequences of sea-ice decline. *Science*, *341*(6145), 519–524.
- Regehr, E. V., Hunter, C. M., Caswell, H., Amstrup, S. C., & Stirling, I. (2010). Survival and breeding of polar bears in the southern beaufort sea in relation to sea ice. *Journal of animal ecology*, *79*(1), 117–127.

- Roosvall, A., & Tegelberg, M. (2015). Media and the geographies of climate justice: Indigenous peoples, nature and the geopolitics of climate change. *tripleC: Communication, Capitalism & Critique. Open Access Journal for a Global Sustainable Information Society*, 13(1), 39–54.
- Serreze, M. C., & Meier, W. N. (2019). The arctic's sea ice cover: trends, variability, predictability, and comparisons to the antarctic. *Annals of the New York Academy of Sciences*, 1436(1), 36–53.
- Stammerjohn, S., Massom, R., Rind, D., & Martinson, D. (2012). Regions of rapid sea ice change: An inter-hemispheric seasonal comparison. *Geophysical Research Letters*, 39(6).
- Zhang, J. (2007). Increasing antarctic sea ice under warming atmospheric and oceanic conditions. *Journal of Climate*, 20(11), 2515–2529.
- Zhang, Z., Nisancioglu, K. H., & Ninnemann, U. S. (2013). Increased ventilation of antarctic deep water during the warm mid-pliocene. *Nature communications*, 4, 1499.